Materials **2015**, *8*, 16-30; doi:10.3390/ma8010016

OPEN ACCESS

materials

ISSN 1996-1944

www.mdpi.com/journal/materials

Article

Photocatalytic Water Splitting for Hydrogen Production with Gd_2MSbO_7 (M = Fe, In, Y) Photocatalysts under Visible Light Irradiation

Jingfei Luan * and Yanyan Li

State Key Laboratory of Pollution Control and Resource Reuse, School of the Environment, Nanjing University, Nanjing 210093, China; E-Mail: mg1325050@smail.nju.edu.cn

* Author to whom correspondence should be addressed; E-Mail: jfluan@nju.edu.cn; Tel./Fax: +86-25-8968-0397.

Academic Editor: Klara Hernadi

Received: 31 October 2014 / Accepted: 18 December 2014 / Published: 24 December 2014

Abstract: Novel photocatalysts Gd_2FeSbO_7, Gd_2InSbO_7 and Gd_2YSbO_7 were synthesized by the solid state reaction method for the first time. A comparative study about the structural and photocatalytic properties of Gd_2MSbO_7 (M = Fe, In, Y) was reported. The results showed that Gd_2FeSbO_7, Gd_2InSbO_7 and Gd_2YSbO_7 crystallized with the pyrochlore-type structure, cubic crystal system and space group Fd3m. The lattice parameter *a* for Gd_2FeSbO_7, Gd_2InSbO_7 or Gd_2YSbO_7 was 10.276026 Å, 10.449546 Å or 10.653651 Å. The band gap of Gd_2FeSbO_7, Gd_2InSbO_7 or Gd_2YSbO_7 was estimated to be 2.151 eV, 2.897 eV or 2.396 eV. For the photocatalytic water-splitting reaction, H_2 or O_2 evolution was observed from pure water with Gd_2FeSbO_7, Gd_2InSbO_7 or Gd_2YSbO_7 as catalyst under visible light irradiation (wavelength > 420 nm). Moreover, H_2 or O_2 also spilt by using Gd_2FeSbO_7, Gd_2InSbO_7 or Gd_2YSbO_7 as catalyst from CH_3OH/H_2O or $AgNO_3/H_2O$ solutions under visible light irradiation (λ > 420 nm). Gd_2FeSbO_7 showed the highest activity compared with Gd_2InSbO_7 or Gd_2YSbO_7. At the same time, Gd_2InSbO_7 showed higher activity compared with Gd_2YSbO_7. The photocatalytic activities were further improved under visible light irradiation with Gd_2FeSbO_7, Gd_2InSbO_7 or Gd_2YSbO_7 being loaded by Pt, NiO or RuO_2. The effect of Pt was better than that of NiO or RuO_2 for improving the photocatalytic activity of Gd_2FeSbO_7, Gd_2InSbO_7 or Gd_2YSbO_7.

Keywords: Gd_2MSbO_7 (M = Fe; In; Y); photocatalytic water splitting; visible light irradiation; photocatalytic property

1. Introduction

Since water splitting reaction with TiO_2 as catalyst was discovered in 1972 [1], photocatalysis, as one energy-conserving and green emerging technology, has been studied massively and in detail for producing renewable hydrogen. However, early photocatalysts were applied conditionally for their ultraviolet light response. In order to make good use of exhaustless solar energy, plenty of endeavors were made to develop visible light responsive photocatalysts. By summarizing recent research achievements, there were mainly two approaches to obtain visible light responsive photocatalysts. The first approach was to modify TiO_2, such as by ion doping [2–4] or forming heterojunction [5–7], which was studied most repeatedly due to its non-toxic performance, excellent stability and low cost. The second approach was to develop new photocatalysts, which had also achieved great progress [8–14]. Especially, the reported CdS photocatalyst [15], with Pt and PdS together as cocatalysts, realized a high quantum efficiency up to 93% in photocatalytic H_2 production, which had aroused wide attention across the world. It was known that TiO_2 could not be used in the visible light region and could only split water under ultraviolet light irradiation. Moreover, ultraviolet light only occupied 4% of sunlight, which was a limitative factor for photocatalytic technology with TiO_2 as the catalyst. Thus, the efficient photocatalysts which could produce electron–hole pairs under visible light irradiation should be developed because visible light occupied 43% of sunlight.

Bi_2MNbO_7 ($M = Fe^{3+}$, In^{3+}) [16] photocatalysts, as one remarkable representation of $A_2B_2O_7$ compound family, were first found to realize H_2 evolution which was obtained from pure H_2O during ultraviolet light irradiation. Thereafter, our research group found that Y_2GaSbO_7 or Y_2GdSbO_7 [17] compound also successfully realized photocatalytic water splitting for hydrogen production under visible light irradiation. Therefore, we could reasonably deduce that the substitution of metallic element in $A_2B_2O_7$ compounds by another suitable metallic element might provide a way to find new photocatalysts which could efficiently catalyze water splitting reaction even under visible light irradiation. In addition, the substitution might result in the lattice O^{2-} and O^- ionosorbed on the surface, which created another way to generate hydroxyl radicals and the highly reactive atomic oxygen species and thus could enhance the photocatalytic activity of solid-solution photocatalysts [18]. Moreover, the substitution of metal ion in $A_2B_2O_7$ compounds would probably affect the energy level and narrow the band gap of the $A_2B_2O_7$ compound. As a result, some impurity energy levels or narrow band gaps which had low band gap energy would promote carrier concentration, and thus led to huge change in photocatalytic properties of photocatalysts [19]. Therefore, we speculated Gd_2FeSbO_7, Gd_2InSbO_7 or Gd_2YSbO_7 catalyst might have phocatalytic potential for water splitting reaction, of which we were more convinced when we found that above novel photocatalysts successfully realized degrading rhodamine B under visible light irradiation [20,21].

In this experiment, we synthesized aforementioned photocatalysts Gd_2MSbO_7 (M = Fe, In, Y) again by a solid-state reaction method. Different from previous studies, Gd_2MSbO_7 (M = Fe, In, Y), herein,

served as photocatalysts for splitting water into hydrogen under visible light irradiation. Meanwhile, the structural, photophysical and photocatalytic properties of photocatalysts Gd_2MSbO_7 (M = Fe, In, Y) were also analyzed more comprehensively.

2. Experimental Section

The novel photocatalysts were synthesized by a solid-state reaction method. Gd_2O_3, In_2O_3, Y_2O_3, Fe_2O_3 and Sb_2O_5 with purity of 99.99% (Sinopharm Group Chemical Reagent Co., Ltd., Shanghai, China) were used as starting materials. All powders were dried at 200 °C for 4 h before synthesis. In order to synthesize Gd_2YSbO_7, the precursors were stoichiometrically mixed, then pressed into small columns and put into an alumina crucible (Shenyang Crucible Co., Ltd., Shenyang, China). Finally, calcination was carried out at 1320 °C for 50 h in an electric furnace (KSL 1700X, Hefei Kejing Materials Technology Co., Ltd., Hefei, China). For the sake of preparing Gd_2FeSbO_7, the precursors were stoichiometrically churned up, subsequently pressed into small columns and put into an alumina crucible. Eventually, calcination was performed at 1250 °C for 65 h in an electric furnace. Similarly, Gd_2InSbO_7 was prepared by calcination at 1320 °C for 65 h. The heating rate of calcination was 0.24 °C/s. The crystal structure of Gd_2FeSbO_7, Gd_2InSbO_7 or Gd_2YSbO_7 was analyzed by the powder X-ray diffraction method (D/MAX-RB, Rigaku Corporation, Tokyo, Japan) with Cu*K*α radiation (λ = 1.54056 Å). The voltage was 40.0 kV and current was 30.0 mA. The data were collected at 295 K with a step-scan procedure in the range of 2θ = 10°–100°. The step interval was 0.02° for Gd_2FeSbO_7 or Gd_2YSbO_7 and the time per step was 1.2 s. The step interval was 0.01° for Gd_2InSbO_7 and the time per step was 1.0 s. The chemical composition of Gd_2FeSbO_7, Gd_2InSbO_7 or Gd_2YSbO_7 was determined by scanning electron microscope-X-ray energy dispersion spectrum (SEM-EDS, LEO 1530VP, LEO Corporation, Krefeld, Germany). The scanning accelerating voltage was 20 kV and linked with an Oxford Instruments X-ray analysis system (Oxford, UK) and X-ray fluorescence spectrometer (XFS, ARL-9800, ARL Corporation, Geneva, Switzerland). The diffuse reflectance spectra of Gd_2FeSbO_7, Gd_2InSbO_7 or Gd_2YSbO_7 was analyzed with an UV-visible spectrophotometer (Lambda 40, Perkin-Elmer Corporation, Waltham, MA, USA) in a UV-Vis diffuse reflectance experiment by the dry-pressed disk samples and $BaSO_4$ was used as the reference material. The surface area of Gd_2FeSbO_7, Gd_2InSbO_7 or Gd_2YSbO_7 was measured by the Brunauer-Emmett-Teller (BET) method (MS-21, Quantachrome Instruments Corporation, Boynton Beach, FL, USA) with N_2 adsorption at liquid nitrogen temperature. All the samples were degassed at 180 °C for 8 h prior to nitrogen adsorption measurements. The BET surface area was determined by a multipoint BET method using the adsorption data in the relative pressure (P/P_0) range of 0.05–0.3. A desorption isotherm was used to determine the pore size distribution by the Barret-Joyner-Halender (BJH) method, assuming a cylindrical pore model. The nitrogen adsorption volume at the relative pressure (P/P_0) of 0.994 was used to determine the pore volume and average pore size.

The photocatalytic water splitting was carried out under visible light irradiation in a gas closed circulation system with an inner-irradiation type reactor (quartz cell). A light source (300 W Xe arc lamp, Beijing Dongsheng Glass Light Source Factory, Beijing, China) with the incident photon flux I_0 of 0.056176 μmol cm^{-2} s^{-1} or 0.078245 μmol cm^{-2} s^{-1} was focused through a shutter window and a 420 nm or 390 nm cut-off filter onto the window face of the cell. The incident photon flux I_0 was

determined by a Ray virtual radiation actinometer (FU 100, silicon ray detector, Thorlabs Corporation, Newton, NJ, USA). According to the measured I_0 values with 420 nm and 390 nm cut-off filter, the percentage of UV light passing 390 nm cut-off filter was estimated to be 28.2%. The gas which evolved was determined with a thermal conductivity detector TCD-based gas chromatograph (6890 N, Agilent Technologies, Tempe, AZ, USA), which was connected to the gas closed circulation system. One gram of catalyst was suspended in 300 mL H_2O under stirrer. Before reaction, the closed gas circulation system and the reaction cell were degassed until O_2 and N_2 could not be detected. Then, about 35 Torr of argon was charged into the system. H_2 evolution reaction was carried out in CH_3OH/H_2O solution (50 mL CH_3OH, 300 mL H_2O) with Pt, NiO or RuO_2-loaded powder as the catalyst.

For H_2 evolution reaction, Pt, NiO or RuO_2 which was loaded on the surface of the catalysts, was prepared. Pt was loaded on the catalyst surface by an *in situ* photodeposition method by using aqueous H_2PtCl_6 solution (Shanghai Chemical Reagent Research Institute, Shanghai, China) as the Pt source. A typical synthesis procedure was as follows: 1 g catalyst powder and a calculated amount of (0.2 wt%) H_2PtCl_6 solution were mixed in 150 mL deionized water, and the suspension was then irradiated by a 300 W Xe lamp ($\lambda > 420$ nm) under continuous stirring. After 5 h photo-deposition, the suspension was filtered, washed with de-ionized water for 4 times, and finally dried in vacuum at 60 °C for 12 h. NiO or RuO_2 which was loaded on the surface of the catalysts, was prepared by the impregnation method by using $Ni(NO_3)_2$ or $RuCl_3$ solution (Sinopharm Group Chemical Reagent Co., Ltd., Shanghai, China), separately. Normally, 1 g catalyst powder was ultrasonically dispersed in 20 mL deionized water, and then a calculated amount of metal precursors (1.0 wt%) $Ni(NO_3)_2$ or $RuCl_3$ solution was added to the catalyst powder dispersed water. After magnetically stirring for 1 h, the mixed solution was boiled at 100 °C, and next dried at 60 °C for 12 h. Lastly, the as obtained sample was put into an electric furnace to calcine for 4 h at 450 °C in moving air.

3. Results and Discussion

3.1. Characterization

Figure 1 shows the X-ray powder diffraction patterns of Gd_2FeSbO_7, Gd_2InSbO_7 and Gd_2YSbO_7. It could be seen from Figure 1 that Gd_2FeSbO_7, Gd_2InSbO_7 or Gd_2YSbO_7 was a single phase. The calculations of lattice parameters were performed with the program of Cambridge serial total energy package (CASTEP) and first-principles simulation. The CASTEP package was provided by Materials Studio software and the CASTEP calculation was composed of the plane-wave pseudopotential total energy method according to the density functional theory. Thus, our calculations were based on the plane-wave-based density functional theory (DFT) in generalized gradient approximations (GGA) with Perdew–Burke–Ernzerh of (PBE) exchange-correlation potential.

In order to obtain the crystal lattice parameters, Rietveld refinement from X-Ray Diffraction (XRD) data was performed with DBWS software, experimental XRD data and simulation XRD data. The uncertainty of the refined lattice parameters lay in the estimated standard deviation (e.s.d.), calculated by the full pattern fitting program. However, e.s.d. was a measure of precision rather than of accuracy, and these two terms must not be confused. For a sound estimation of the measurement uncertainty of lattice parameters that were refined from XRD data, more information was needed than just the e.s.d.

that was provided by the Rietveld refinement of the diffraction pattern of the sample. The outcome of refinements for Gd_2InSbO_7 generated the unweighted *R* factors, R_p = 12.13% with space group Fd3m. As for Gd_2YSbO_7, R_p was 12.16% with space group Fd3m. As for Gd_2FeSbO_7, R_p was 16.20% with space group Fd3m. According to the Rietveld analysis, Gd_2FeSbO_7, Gd_2InSbO_7 or Gd_2YSbO_7 had the pyrochlore-type structure and a cubic crystal system which owned a space group Fd3m. The atomic coordinates and structural parameters of Gd_2FeSbO_7, Gd_2InSbO_7 and Gd_2YSbO_7 are listed in Tables 1–3, respectively. The lattice parameter *a* for Gd_2FeSbO_7, Gd_2InSbO_7 or Gd_2YSbO_7 was 10.276026 Å, 10.449546 Å or 10.653651 Å. Moreover, the XRD results showed that two theta angles of each reflection of Gd_2FeSbO_7 changed with Fe^{3+} being substituted by In^{3+} or Y^{3+}. The lattice parameter α increased from α = 10.276026 Å for Gd_2FeSbO_7 to α = 10.449546 Å for Gd_2InSbO_7, which indicated a decrease in the lattice parameter of the photocatalyst with a decrease of the M ionic radii, Fe^{3+} (0.78 Å) < In^{3+} (0.92 Å). The lattice parameter α also increased from α = 10.276026 Å for Gd_2FeSbO_7 to α = 10.653651 Å for Gd_2YSbO_7, which indicated a decrease in lattice parameter of the photocatalyst with decrease of the M ionic radii, Fe^{3+} (0.78 Å) < Y^{3+} (1.019 Å). Meanwhile, The lattice parameter α also increased from α = 10.449546 Å for Gd_2InSbO_7 to α = 10.653651 Å for Gd_2YSbO_7, which indicated a decrease in the lattice parameter of the photocatalyst with a decrease of the M ionic radii, In^{3+} (0.92 Å) < Y^{3+} (1.019 Å).

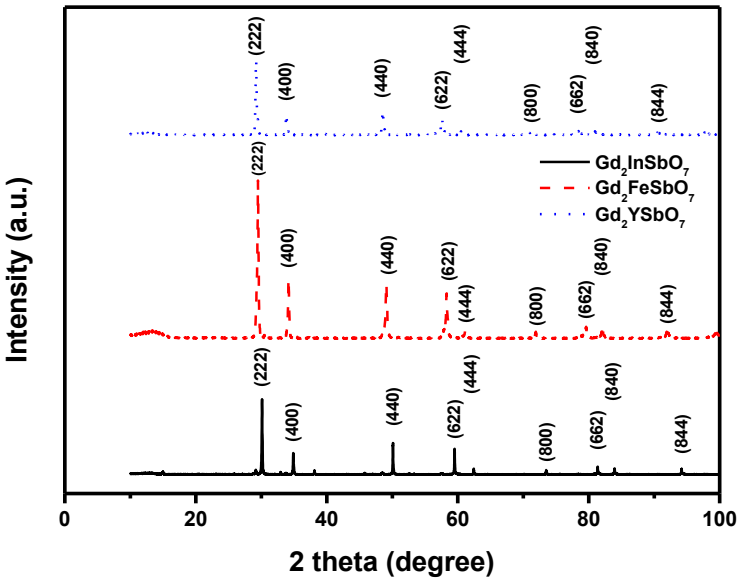

Figure 1. X-ray powder diffraction pattern of Gd_2FeSbO_7, Gd_2InSbO_7 or Gd_2YSbO_7 prepared by a solid-state reaction method at 1250 °C, 1320 °C or 1320 °C.

Table 1. Structural parameters of Gd_2YSbO_7 prepared by solid-state reaction method. *x*, *y* and *z* refer to the position coordinates of different atoms in one unit cell, respectively.

Atom	*x*	*y*	*z*	Occupation Factor
Gd	0.00000	0.00000	0.00000	1.0
Y	0.50000	0.50000	0.50000	0.5
Sb	0.50000	0.50000	0.50000	0.5
O(1)	−0.16519	0.12500	0.12500	1.0
O(2)	0.12500	0.12500	0.12500	1.0

Table 2. Structural parameters of Gd_2BiSbO_7 prepared by solid-state reaction method. *x*, *y* and *z* refer to the position coordinates of different atoms in one unit cell, respectively.

Atom	*x*	*y*	*z*	Occupation Factor
Gd	0.00000	0.00000	0.00000	1.0
Bi	0.50000	0.50000	0.50000	0.5
Sb	0.50000	0.50000	0.50000	0.5
O(1)	−0.14538	0.12500	0.12500	1.0
O(2)	0.12500	0.12500	0.12500	1.0

Table 3. Structural parameters of Gd_2FeSbO_7 prepared by solid-state reaction method. *x*, *y* and *z* refer to the position coordinates of different atoms in one unit cell, respectively.

Atom	*x*	*y*	*z*	Occupation Factor
Gd	0.00000	0.00000	0.00000	1.0
Fe	0.50000	0.50000	0.50000	0.5
Sb	0.50000	0.50000	0.50000	0.5
O(1)	−0.20249	0.12500	0.12500	1.0
O(2)	0.12500	0.12500	0.12500	1.0

Figure 2 represents the diffuse reflection spectra of Gd_2FeSbO_7, Gd_2InSbO_7 and Gd_2YSbO_7. Compared with well-known photocatalyst TiO_2 whose absorption edge was only 380 nm, the absorption band edge of Gd_2FeSbO_7, Gd_2InSbO_7 or Gd_2YSbO_7 was found to be 586 nm, 428 nm or 479 nm. Clearly, the obvious absorption did not result from reflection and scattering. Consequently, the apparent absorbance at sub-band gap wavelengths (600–800 nm for Gd_2FeSbO_7, and 425–800 nm for Gd_2InSbO_7, and 490–700 nm for Gd_2YSbO_7) was higher than zero.

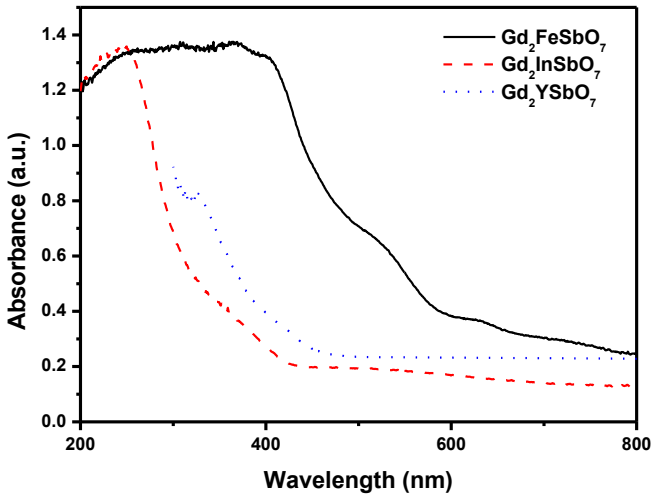

Figure 2. The diffuse reflection spectrum of Gd_2FeSbO_7, Gd_2InSbO_7 or Gd_2YSbO_7.

For a crystalline semiconductor, the optical absorption near the band edge followed the equation: $\alpha h\nu = A\ (h\nu - E_g)^n$ [22,23]. Here, *A*, α, E_g and ν were proportional constant, absorption coefficient, band gap and light frequency, respectively. E_g and *n* could be calculated by the following steps: (i) plotting $\ln(\alpha h\nu)$ *vs.* $\ln(h\nu - E_g)$ by assuming an approximate value of E_g; (ii) deducing the value of *n* according to the slope in this graph; (iii) refining the value of E_g by plotting $(\alpha h\nu)^{1/n}$ *vs.* $h\nu$ and

extrapolating the plot to $(\alpha h\nu)^{1/n} = 0$. According to the above method, the band gap of Gd_2FeSbO_7, Gd_2InSbO_7 or Gd_2YSbO_7 was estimated to be 2.151 eV, 2.897 eV or 2.396 eV.

3.2. Photocatalytic Activity of Gd_2FeSbO_7, Gd_2InSbO_7 and Gd_2YSbO_7

Generally speaking, the semiconductor photocatalysis started from the direct absorption of supra-band gap photons and the generation of electron–hole pairs in the semiconductor particles. Subsequently, the diffusion of the charge carriers to the surface of the semiconductor particle was followed. Under visible light irradiation, we measured H_2 or O_2 evolution rate by using Gd_2FeSbO_7, Gd_2InSbO_7 or Gd_2YSbO_7 as photocatalyst from CH_3OH/H_2O or $AgNO_3/H_2O$ solution, respectively. The wavelength (λ) dependence on the photocatalytic activity under light irradiation from full arc up to λ = 420 nm was measured by using different cut-off filters.

Figure 3a shows the photocatalytic H_2 evolution from pure water with Gd_2FeSbO_7, Gd_2InSbO_7 or Gd_2YSbO_7 as catalyst under visible light irradiation (λ > 420 nm, 0.5 g powder sample, 250 mL pure water). It could be found from Figure 3a that under visible light irradiation, the rate of H_2 evolution in the first 28 h with Gd_2FeSbO_7 as catalyst was 6.329 μmol h^{-1} g^{-1}, and that with Gd_2InSbO_7 as catalyst was 5.157 μmol h^{-1} g^{-1}, and that with Gd_2YSbO_7 as catalyst was 4.314 μmol h^{-1} g^{-1}. Besides, under dark condition, no H_2 evolution was detected from pure water with above three catalysts, which reflected the phocatalytic H_2 evolution activities from pure water of three synthesized catalysts. The reason that water could be split for H_2 evolution from pure water with Gd_2FeSbO_7, Gd_2InSbO_7 or Gd_2YSbO_7 as catalyst under visible light irradiation (λ > 420 nm) was as following: Water could be split at a wavelength higher than 420 nm. However, the wavelength was not cut in exactly at 420 nm, in fact, the wavelength was cut by +50 or −50 nm, which meant that the wavelength up to 370 nm was probably absorbed by Gd_2FeSbO_7, Gd_2InSbO_7 or Gd_2YSbO_7, which could split water to provide tiny amounts of hydrogen generation in our experiment. The recycling experiments were performed three times with the same experimental conditions of Figure 3a, and the results were almost the same as the above results in Figure 3a. It could be seen that the photocatalysts we had produced had good stability and were thus desirably recyclable.

Figure 3b shows the photocatalytic O_2 evolution from pure water with Gd_2FeSbO_7, Gd_2InSbO_7 or Gd_2YSbO_7 as catalyst under visible light irradiation (λ > 420 nm, 0.5 g powder sample, 250 mL pure water). It could be found from Figure 3b that under visible light irradiation, the rate of O_2 evolution in the first 28 h with Gd_2FeSbO_7 as catalyst was 3.158 μmol h^{-1} g^{-1}, and that with Gd_2InSbO_7 as catalyst was 2.574 μmol h^{-1} g^{-1}, and that with Gd_2YSbO_7 as catalyst was 2.149 μmol h^{-1} g^{-1}.

Figure 3c shows the photocatalytic H_2 evolution from aqueous methanol solution with Gd_2FeSbO_7, Gd_2InSbO_7 or Gd_2YSbO_7 as catalyst under visible light irradiation (λ > 420 nm, 0.5 g 0.1 wt% Pt-loaded powder sample, 50 mL methanol solution, 200 mL pure water). It could be found from Figure 3c that under visible light irradiation, the rate of H_2 evolution in the first 28 h with Gd_2FeSbO_7 as catalyst was 18.271 μmol h^{-1} g^{-1}, and that with Gd_2InSbO_7 as catalyst was 12.479 μmol h^{-1} g^{-1}, and that with Gd_2YSbO_7 as catalyst was 10.986 μmol h^{-1} g^{-1}, indicating that the photocatalytic activity of Gd_2FeSbO_7 was much higher than that of Gd_2InSbO_7 or Gd_2YSbO_7.

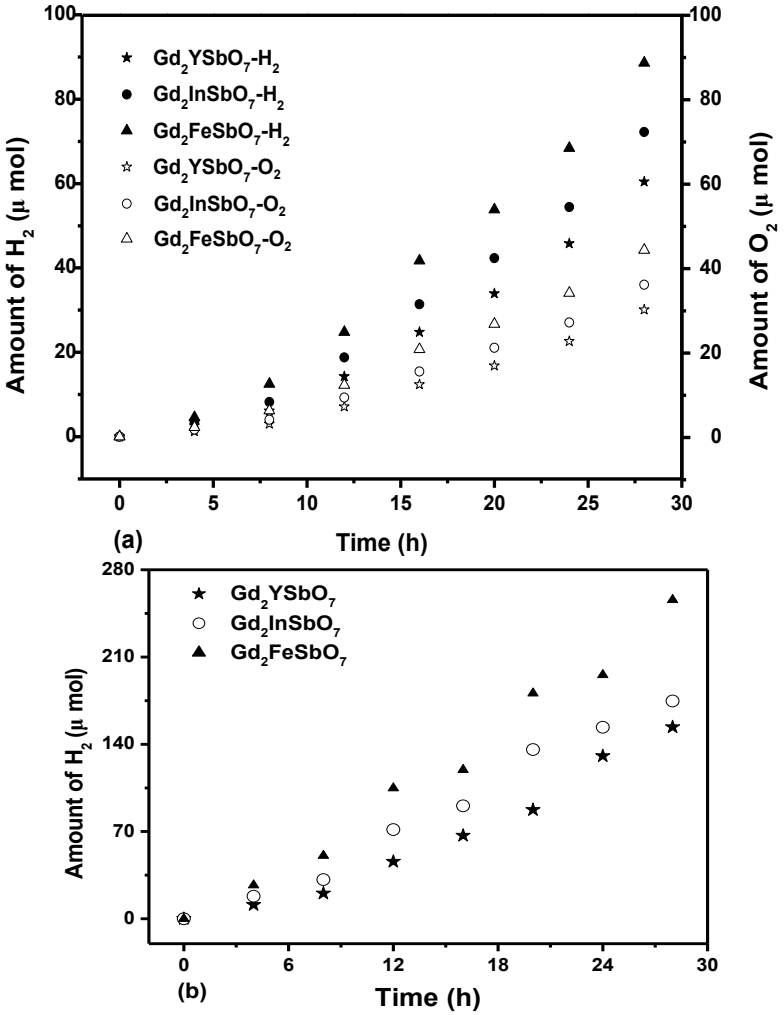

Figure 3. (**a**) Photocatalytic H_2 evolution and photocatalytic O_2 evolution from pure water with Gd_2FeSbO_7, Gd_2InSbO_7 or Gd_2YSbO_7 as catalyst under visible light irradiation ($\lambda > 420$ nm, 0.5 g powder sample, 250 mL pure water). Light source: 300 W Xe lamp; (**b**) Photocatalytic H_2 evolution from aqueous methanol solution with Gd_2FeSbO_7, Gd_2InSbO_7 or Gd_2YSbO_7 as catalyst under visible light irradiation ($\lambda > 420$ nm, 0.5 g 0.1 wt% Pt-loaded powder sample, 50 mL methanol solution, 200 mL pure water). Light source: 300 W Xe lamp.

We would estimate apparent quantum yield in this paper because scattering effects were assumed to be the same for all the photocatalysts and our system was a suspension rather than a homogeneous solution. The apparent quantum yield for hydrogen evolution at 420 nm with Gd_2FeSbO_7 as catalyst was 0.446%, and that with Gd_2InSbO_7 as catalyst was 0.305% and that with Gd_2YSbO_7 as catalyst was 0.268% under visible light irradiation. Moreover, Gd_2InSbO_7 showed higher photocatalytic activity than Gd_2YSbO_7. This also proved that the conduction band level of Gd_2FeSbO_7, Gd_2InSbO_7 or Gd_2YSbO_7 was more negative than the reduction potential of H_2O for forming H_2. The formation rate of H_2 increased with decreasing the M ionic radii within Gd_2MSbO_7 (M = Fe, In, Y), Fe^{3+} (0.78 Å) < In^{3+} (0.92 Å) < Y^{3+} (1.019 Å). The reason was that the surface area of the photocatalyst increased with decreasing the M ionic radii, and the creation of more active sites was realized. As a result, the hydrogen generation rate increased. Moreover, the decrease of the M ionic radii would result

in a decrease for the migration distance of photogenerated electrons and holes to reach the reaction site on the photocatalyst surface. Thus, the photogenerated electrons and holes could get to the photocatalyst surface more quickly. Above factors would suppress the electron–hole recombination, therefore, the photocatalytic activity would be enhanced. Such results were in good agreement with the optical absorption property of Gd_2FeSbO_7, Gd_2InSbO_7 or Gd_2YSbO_7 (see Figure 2). The rate of H_2 evolution also increased with increasing illumination time. The photocatalytic activity of Gd_2FeSbO_7 increased by about 166% than that of Gd_2YSbO_7.

Figure 4 shows the photocatalytic O_2 evolution from $AgNO_3$ solution with Gd_2FeSbO_7, Gd_2InSbO_7 or Gd_2YSbO_7 as catalyst under visible light irradiation ($\lambda > 420$ nm, 0.5 g photocatalyst, 1 mmol $AgNO_3$, 270 mL pure water). It could be seen from Figure 4 that under visible light irradiation, the rate of O_2 evolution in the first 28 h with Gd_2FeSbO_7 as catalyst was 34.329 μmol h^{-1} g^{-1}, and that with Gd_2InSbO_7 as catalyst was 23.264 μmol h^{-1} g^{-1}, and that with Gd_2YSbO_7 as catalyst was 17.200 μmol $h^{-1}g^{-1}$, indicating that the valence band level of Gd_2FeSbO_7, Gd_2InSbO_7 or Gd_2YSbO_7 was more positive than the oxidation potential of H_2O for forming O_2. The formation rate of O_2 increased with decreasing the M ionic radii within Gd_2MSbO_7 (M = Fe, In, Y), Fe^{3+} (0.78 Å) < In^{3+} (0.92 Å) < Y^{3+} (1.019 Å). The apparent quantum yield for the oxygen evolution at 420 nm with Gd_2FeSbO_7 as catalyst was 1.677%, and that with Gd_2InSbO_7 as catalyst was 1.136%, and that with Gd_2YSbO_7 as catalyst is 0.840% under visible light irradiation.

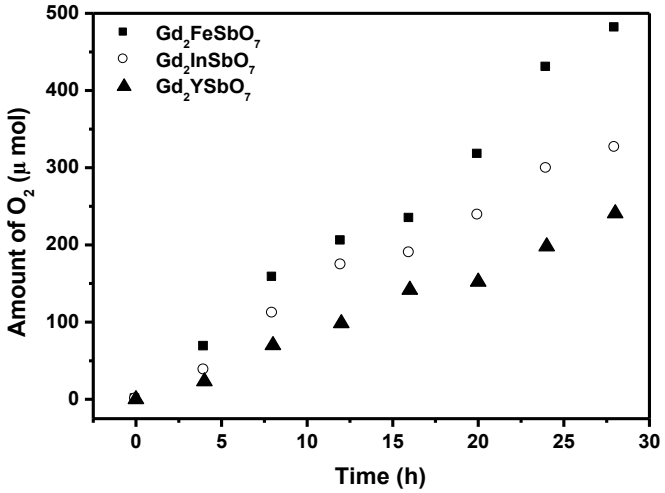

Figure 4. Photocatalytic O_2 evolution from $AgNO_3$ solution with Gd_2FeSbO_7, Gd_2InSbO_7 or Gd_2YSbO_7 as catalyst under visible light irradiation ($\lambda > 420$ nm, 0.5 g photocatalyst, 1 mmol $AgNO_3$, 270 mL pure water). Light source: 300 W Xe lamp.

Figure 5 shows the photocatalytic H_2 evolution from aqueous methanol solution with Gd_2FeSbO_7, Gd_2InSbO_7 or Gd_2YSbO_7 as catalyst under light irradiation (390 nm cut-off filter, 0.5 g 0.1 wt% Pt-loaded powder sample, 50 mL CH_3OH, 200 mL pure water). It was depicted in Figure 5 that under light irradiation (390 nm cut-off filter), the rate of H_2 evolution in the first 28 h with Gd_2FeSbO_7 as catalyst was 49.707 μmol h^{-1} g^{-1}, and that with Gd_2InSbO_7 as catalyst was 35.900 μmol h^{-1} g^{-1}, and that with Gd_2YSbO_7 as catalyst was 29.457 μmol h^{-1} g^{-1}, indicating that the effect of wavelength (λ) dependence on the photocatalytic activity was very important. The apparent quantum yield for hydrogen evolution at 390 nm with Gd_2FeSbO_7 as catalyst was 0.871%, and that with Gd_2InSbO_7 as

catalyst was 0.629% and that with Gd_2YSbO_7 as catalyst was 0.516% under light irradiation (390 nm cut-off filter).

The photocatalytic H_2 evolution from aqueous methanol solution with Gd_2FeSbO_7, Gd_2InSbO_7 or Gd_2YSbO_7 as catalyst under light irradiation (No cut-off filter, 0.5 g 0.1 wt% Pt-loaded powder sample, 50 mL CH_3OH, 200 mL pure water) are shown in Figure 6. It could be found from Figure 6 that under light irradiation without using any filters, the rate of H_2 evolution in the first 28 h with Gd_2FeSbO_7 as catalyst was 94.614 μmol h^{-1} g^{-1}, and that with Gd_2InSbO_7 as catalyst was 70.893 μmol h^{-1} g^{-1}, and that with Gd_2YSbO_7 as catalyst was 57.100 μmol h^{-1} g^{-1}, indicating that Gd_2FeSbO_7, Gd_2InSbO_7 or Gd_2YSbO_7 shows high photocatalytic activity under full arc irradiation. The apparent quantum yield for hydrogen evolution at 420 nm with Gd_2FeSbO_7 as catalyst was 2.311%, and that with Gd_2InSbO_7 as catalyst was 1.731%, and that with Gd_2YSbO_7 as catalyst was 1.394% under light irradiation without using any filters. The photocatalytic activity decreased with increasing incident wavelength λ. As to Gd_2FeSbO_7, Gd_2InSbO_7 or Gd_2YSbO_7, the turnover number—the ratio of total amount of gas evolves to catalyst—exceeded 1 for Gd_2FeSbO_7 after 46 h reaction time, exceeded 1 for Gd_2InSbO_7 after 57 h reaction time, and exceeded 1 for Gd_2YSbO_7 after 66 h reaction time under visible light irradiation (λ > 420 nm). Under the condition of full arc irradiation, after 28 h of reaction time, the turnover number exceeded 1.60 for Gd_2FeSbO_7, and the turnover number exceeded 1.32 for Gd_2InSbO_7, and the turnover number exceeded 1.02 as to Gd_2YSbO_7. Above results were enough to prove that the reaction occurred catalytically. The reaction stopped when the light was turned off in this experiment, showing the obvious light response.

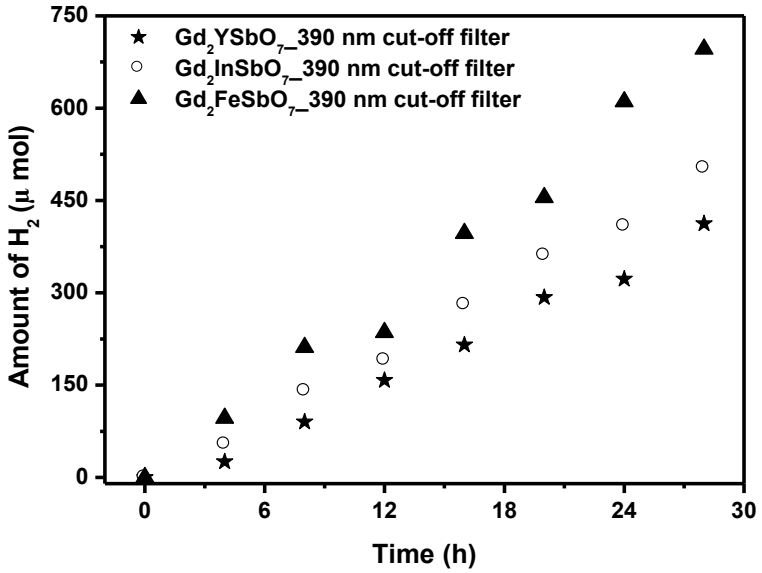

Figure 5. Photocatalytic H_2 evolution from aqueous methanol solution with Gd_2FeSbO_7, Gd_2InSbO_7 or Gd_2YSbO_7 as catalyst under light irradiation (390 nm cut-off filter, 0.5 g 0.1 wt% Pt-loaded powder sample, 50 mL CH_3OH, 200 mL pure water). Light source: 300 W Xe lamp.

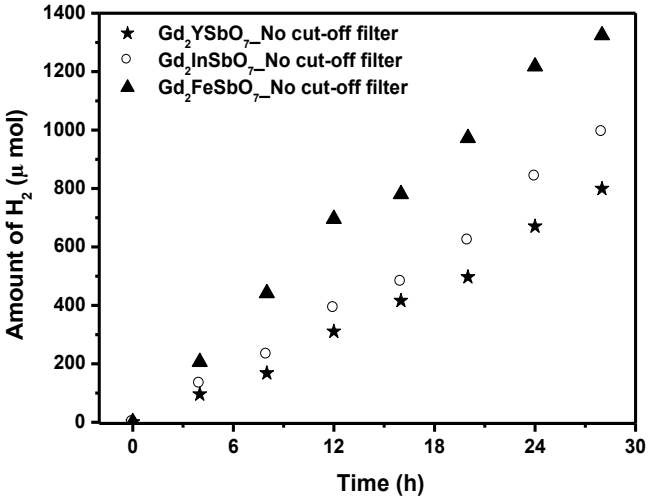

Figure 6. Photocatalytic H_2 evolution from aqueous methanol solution with Gd_2FeSbO_7, Gd_2InSbO_7 or Gd_2YSbO_7 as catalyst under light irradiation (No cut-off filter, 0.5 g 0.1 wt% Pt-loaded powder sample, 50 mL CH_3OH, 200 mL pure water). Light source: 300 W Xe lamp.

It was known that TiO_2 has very high photocatalytic activity under ultraviolet light irradiation. By contrast, the photocatalytic activity was not obtained with Pt/TiO_2 as catalyst under visible light irradiation ($\lambda > 420$ nm), while an obvious photocatalytic activity was observed with Gd_2FeSbO_7, Gd_2InSbO_7 or Gd_2YSbO_7 as catalyst, showing that Gd_2FeSbO_7, Gd_2InSbO_7 or Gd_2YSbO_7 could respond to visible light irradiation. The formation rate of H_2 evolution with Gd_2FeSbO_7, Gd_2InSbO_7 or Gd_2YSbO_7 as catalyst was much larger than that with TiO_2 as catalyst under visible light irradiation. This indicated that the photocatalytic activity of Gd_2FeSbO_7, Gd_2InSbO_7 or Gd_2YSbO_7 for decomposing CH_3OH/H_2O solution was higher than that of TiO_2. The structure of Gd_2FeSbO_7, Gd_2InSbO_7 or Gd_2YSbO_7 after photocatalytic reaction was also checked by using X-ray diffraction method, and no change in their structures was observed during this reaction, which indicated that the H_2 evolution was induced from the photocatalytic reaction of H_2O.

Figure 7 shows the effect of Pt, NiO and RuO_2 co-catalysts on the photoactivity of Gd_2FeSbO_7 under visible light irradiation ($\lambda > 420$ nm, 0.5 g powder sample, 50 mL methanol solution, 200 mL pure water). In principle, the photoinduced electrons preferentially enriched on the surface of co-catalyst particles and the recombination of the photoinduced electrons with the photoinduced holes was therefore markedly suppressed. It could be found from Figure 7 that in the first 28 h under visible light irradiation, the rate of H_2 evolution was estimated to be 41.471 μmol h^{-1} g^{-1} with 0.2 wt%-Pt/Gd_2FeSbO_7 as catalyst, and that was estimated to be 32.064 μmol h^{-1} g^{-1} with 1.0 wt%-NiO/Gd_2FeSbO_7 as catalyst, and that was estimated to be 24.114 μmol h^{-1} g^{-1} with 1.0 wt%-RuO_2/Gd_2FeSbO_7 as catalyst, indicating that the photocatalytic activities could be further improved under visible light irradiation with Gd_2FeSbO_7, Gd_2InSbO_7 or Gd_2YSbO_7 being loaded by Pt, NiO or RuO_2. The apparent quantum yield for hydrogen evolution at 420 nm with 0.2 wt%-Pt/Gd_2FeSbO_7 as catalyst was 1.013%, and that with 1.0 wt%-NiO/Gd_2FeSbO_7 as catalyst was 0.783%, and that with 1.0 wt%-RuO_2/Gd_2FeSbO_7 as catalyst was 0.589% under visible light irradiation ($\lambda > 420$ nm). The effect of Pt was better than that of NiO or RuO_2 for improving the photocatalytic activity of Gd_2FeSbO_7, Gd_2InSbO_7 or Gd_2YSbO_7.

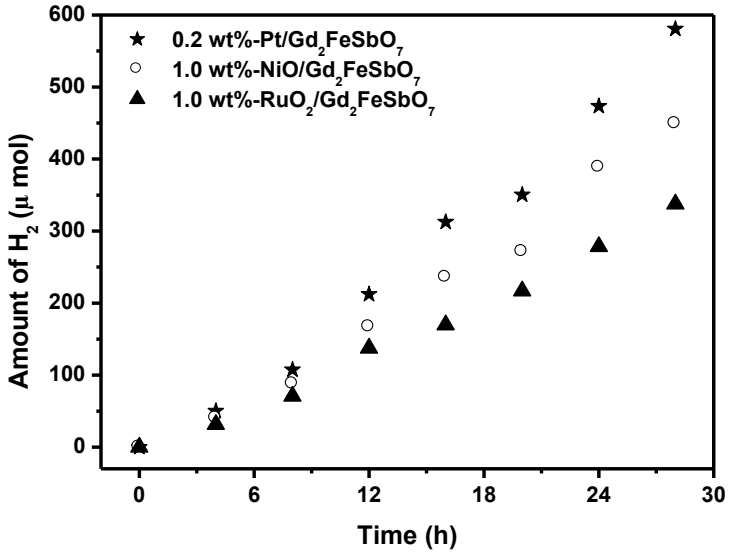

Figure 7. Effect of Pt, NiO and RuO_2 co-catalysts on the photoactivity of Gd_2FeSbO_7 under visible light irradiation ($\lambda > 420$ nm, 0.5 g powder sample, 50 mL methanol solution, 200 mL pure water). Light source: 300 W Xe lamp.

It was known that the process for photocatalysis of semiconductors was the direct absorption of photon by band gap of the materials and generated electron–hole pairs in the semiconductor particles, and the excitation of an electron from the valence band to the conduction band was initiated by light absorption with energy equal to or greater than the band gap of the semiconductor. Upon excitation of photon, the separated electron and hole could follow the solid surface. This suggested that the narrow band gap could more easily excite an electron from the valence band to the conduction band. If the conduction band potential level of the semiconductor was more negative than that of H_2 evolution, and the valence band potential level was more positive than that of O_2 evolution, decomposition of water could occur even without applying electric power [1]. According to the above analysis, the photon absorption of Gd_2FeSbO_7 was much easier than that of the Gd_2InSbO_7 or Gd_2YSbO_7, which resulted in higher photocatalytic activity of Gd_2FeSbO_7.

The information about the specific surface area, pore volume, average pore size of Gd_2FeSbO_7, Gd_2InSbO_7 and Gd_2YSbO_7 are presented in Table 4, from which we could see that the specific surface area of Gd_2FeSbO_7, Gd_2InSbO_7 or Gd_2YSbO_7 was measured to be 4.12 $m^2\ g^{-1}$, 3.26 $m^2\ g^{-1}$ or 1.28 $m^2\ g^{-1}$, which was significantly smaller than that of TiO_2 photocatalyst (53.8 $m^2\ g^{-1}$). Above results indicated much higher potential efficiency of Gd_2FeSbO_7, Gd_2InSbO_7 or Gd_2YSbO_7. Although the surface area of Gd_2FeSbO_7, Gd_2InSbO_7 or Gd_2YSbO_7 was smaller than that of TiO_2, but Gd_2FeSbO_7, Gd_2InSbO_7 or Gd_2YSbO_7 showed higher photocatalytic activity for H_2 evolution under visible light irradiation, which indicated that the high photocatalytic activity of the Gd_2FeSbO_7, Gd_2InSbO_7 or Gd_2YSbO_7 was not owing to a big surface area, but rather due to the narrow band gap. It was obvious that further increase in photocatalytic activity might be prospected from increasing the surface area of Gd_2FeSbO_7, Gd_2InSbO_7 or Gd_2YSbO_7. Since an efficient photocatalytic reaction process occurred on the photocatalyst surface, the increase of the surface area for the photocatalysts might lead to the increase of their photocatalytic activity.

Table 4. The detailed information about the specific surface area, pore volume, average pore size of Gd_2FeSbO_7, Gd_2InSbO_7 and Gd_2YSbO_7 catalysts.

Catalyst	Specific Surface Area (m^2 g^{-1})	Pore Volume (cm^3 g^{-1})	Average Pore Size (nm)
Gd_2FeSbO_7	4.12	0.034	33
Gd_2InSbO_7	3.26	0.033	41
Gd_2YSbO_7	1.28	0.019	59

4. Conclusions

In the present work, we prepared single phase of Gd_2FeSbO_7, Gd_2InSbO_7 or Gd_2YSbO_7 by solid-state reaction method and studied the structural, optical and photocatalytic properties of Gd_2FeSbO_7, Gd_2InSbO_7 or Gd_2YSbO_7. Rietveld structure refinement results revealed that Gd_2FeSbO_7, Gd_2InSbO_7 or Gd_2YSbO_7 crystallized with the pyrochlore-type structure, cubic crystal system and space group Fd3m. The lattice parameter *a* for Gd_2FeSbO_7, Gd_2InSbO_7 or Gd_2YSbO_7 was 10.276026 Å, 10.449546 Å or 10.653651 Å. The band gap of Gd_2FeSbO_7, Gd_2InSbO_7 or Gd_2YSbO_7 was estimated to be 2.151 eV, 2.897 eV or 2.396 eV. Gd_2FeSbO_7, Gd_2InSbO_7 or Gd_2YSbO_7 showed optical absorption in the visible light region, indicating that above photocatalysts had the ability to respond to the wavelength of visible light region. For the photocatalytic water-splitting reaction, H_2 or O_2 evolution was observed from pure water with Gd_2FeSbO_7, Gd_2InSbO_7 or Gd_2YSbO_7 as catalyst under visible light irradiation ($\lambda > 420$ nm). In addition, under visible light irradiation ($\lambda > 420$ nm), H_2 or O_2 was also produced by using Gd_2FeSbO_7, Gd_2InSbO_7 or Gd_2YSbO_7 as catalyst from CH_3OH/H_2O or $AgNO_3/H_2O$ solutions. Gd_2FeSbO_7 showed the highest activity compared with Gd_2InSbO_7 or Gd_2YSbO_7. At the same time, Gd_2InSbO_7 showed higher activity compared with Gd_2YSbO_7. The photocatalytic activities were further improved under visible light irradiation with Gd_2FeSbO_7 being loaded by Pt, NiO or RuO_2. The effect of Pt was better than that of NiO or RuO_2 for improving the photocatalytic activity of Gd_2FeSbO_7. Moreover, the synthesis of Gd_2FeSbO_7, Gd_2InSbO_7 or Gd_2YSbO_7 offered some useful insights for the design of new photocatalysts for the photocatalytic evolution of H_2 or O_2.

Acknowledgments

This work was supported by the National Natural Science Foundation of China (No. 21277067). This work was supported by a grant from China-Israel Joint Research Program in Water Technology and Renewable Energy (No. 5). This work was supported by a grant from the Natural Science Foundation of Jiangsu Province (No. BK20141312). This work was supported by a Project of Science and Technology Development Plan of Suzhou City of China from 2014 (No. ZXG201440). This work was supported by a grant from the Fundamental Research Funds for the Central Universities.

Author Contributions

Jingfei Luan conceived and designed the experiment project. Yanyan Li performed the experiments. Jingfei Luan and Yanyan Li wrote the paper. All authors read and approved the manuscript.

Conflicts of Interest

The authors declare no conflict of interest.

References

1. Fujishima, A.; Honda, K. Electrochemical photolysis of water at a semiconductor electrode. *Nature* **1972**, *238*, 37–38.
2. Babu, V.J.; Kumar, M.K.; Nair, A.S.; Kheng, T.L.; Allakhverdiev, S.I.; Ramakrishna, S. Visible light photocatalytic water splitting for hydrogen production from N-TiO_2 rice grain shaped electrospun nanostructures. *Int. J. Hydrog. Energy* **2012**, *37*, 8897–8904.
3. Niishiro, R.; Kato, H.; Kudo, A. Nickel and either tantalum or niobium-codoped TiO_2 and $SrTiO_3$ photocatalysts with visible-light response for H_2 or O_2 evolution from aqueous solutions. *Phys. Chem. Chem. Phys.* **2005**, *7*, 2241–2245.
4. Zuo, F.; Wang, L.; Feng, P.Y. Self-doped Ti^{3+}@TiO_2 visible light photocatalyst: Influence of synthetic parameters on the H_2 production activity. *Int. J. Hydrog. Energy* **2014**, *39*, 711–717.
5. Qu, Y.; Zhou, W.; Ren, Z.Y.; Tian, C.G.; Li, J.L.; Fu, H.G. Heterojunction Ag–TiO_2 nanopillars for visible-light-driven photocatalytic H_2 production. *ChemPlusChem* **2014**, *79*, 995–1000.
6. Reddy, P.A.K.; Srinivas, B.; Kumari, V.D.; Shankar, M.V.; Subrahmanyam, M.; Lee, J.S. $CaFe_2O_4$ sensitized hierarchical TiO_2 photo composite for hydrogen production under solar light irradiation. *Chem. Eng. J.* **2014**, *247*, 152–160.
7. Yan, J.H.; Zhu, Y.R.; Tang, Y.G.; Yang, H.H. Preparation and photocatalytic activity for H_2 production over Pt/$SrZr_{0.95}Y_{0.05}O_3TiO_{2-x}N_x$ composite catalyst under simulated sunlight irradiation. *Chin. J. Inorg. Chem.* **2008**, *24*, 791–796.
8. Ding, J.J.; Sun, S.; Yan, W.H.; Bao, J.; Gao, C. Photocatalytic H_2 evolution on a novel $CaIn_2S_4$ photocatalyst under visible light irradiation. *Int. J. Hydrog. Energy* **2013**, *38*, 13153–13158.
9. Gupta, U.; Rao, B.G.; Maitra, U.; Prasad, B.E.; Rao, C.N.R. Visible-light-induced generation of H_2 by nanocomposites of few-layer TiS_2 and TaS_2 with CdS nanoparticles. *Chem. Asian J.* **2014**, *9*, 1311–1315.
10. Yang, M.Q.; Weng, B.; Xu, Y.J. Improving the visible light photoactivity of In_2S_3-graphene nanocomposite via a simple surface charge modification approach. *Langmuir* **2013**, *29*, 10549–10558.
11. Zhang, J.; Yu, J.G.; Zhang, Y.M.; Li, Q.; Gong, J.R. Visible light photocatalytic H_2 production activity of CuS/ZnS porous nanosheets based on photoinduced interfacial charge transfer. *Nano Lett.* **2011**, *11*, 4774–4779.
12. Zhang, X.H.; Jing, D.W.; Liu, M.C.; Guo, L.J. Efficient photocatalytic H_2 production under visible light irradiation over Ni doped $Cd_{1-x}Zn_xS$ microsphere photocatalysts. *Catal. Commun.* **2008**, *9*, 1720–1724.
13. Zong, X.; Yan, H.J.; Wu, G.P.; Ma, G.J.; Wen, F.Y.; Wang, L.; Li, C. Enhancement of photocatalytic H_2 evolution on CdS by loading MOS_2 as cocatalyst under visible light irradiation. *J. Am. Chem. Soc.* **2008**, *130*, 7176–7177.

14. Zhou, C.; Zhao, Y.F.; Shang, L.; Cao, Y.H.; Wu, L.Z.; Tung, C.H.; Zhang, T.R. Facile preparation of black Nb^{4+} self-doped $K_4Nb_6O_{17}$ microspheres with high solar absorption and enhanced photocatalytic activity. *Chem. Commun.* **2014**, *50*, 9554–9556.
15. Yan, H.J.; Yang, J.H.; Ma, G.J.; Wu, G.P.; Zong, X.; Lei, Z.B.; Shi, J.Y.; Li, C. Visible-light-driven hydrogen production with extremely high quantum efficiency on Pt–PdS/CdS photocatalyst. *J. Catal.* **2009**, *266*, 165–168.
16. Zou, Z.G.; Ye, J.H.; Arakawa, H. Substitution effects of In^{3+} by Fe^{3+} on photocatalytic and structural properties of Bi_2InNbO_7 photocatalysts. *J. Mol. Catal. A Chem.* **2001**, *168*, 289–297.
17. Luan, J.F.; Chen, J.H. Photocatalytic water splitting for hydrogen production with novel Y_2MSbO_7 (M = Ga, In, Gd) under visible light irradiation. *Materials* **2012**, *5*, 2423–2438.
18. Huang, Y.; Zheng, Z.; Ai, Z.H.; Zhang, L.Z.; Fan, X.X.; Zou, Z.G. Core-shell microspherical $Ti_{1-x}Zr_xO_2$ solid solution photocatalysts directly from ultrasonic spray pyrolysis. *J. Phys. Chem. B* **2006**, *110*, 19323–19328.
19. Tang, J.W.; Zou, Z.G.; Yin, J.; Ye, J. Photocatalytic degradation of methylene blue on $CaIn_2O_4$ under visible light irradiation. *Chem. Phys. Lett.* **2003**, *382*, 175–179.
20. Luan, J.F.; Ma, K.; Pan, B.C.; Li, Y.M.; Wu, X.S.; Zou, Z.G. Synthesis and catalytic activity of new Gd_2BiSbO_7 and Gd_2YSbO_7 nanocatalysts. *J. Mol. Catal. A Chem.* **2010**, *321*, 1–9.
21. Luan, J.F.; Xu, Y. Photophysical property and photocatalytic activity of new Gd_2InSbO_7 and Gd_2FeSbO_7 compounds under visible light irradiation. *Int. J. Mol. Sci.* **2013**, *14*, 999–1021.
22. Tauc, J.; Grigorovici, R.; Vancu, A. Optical properties and electronic structure of amorphous germanium. *Phys. Status Solid* **1966**, *15*, 627–637.
23. Butler, M. Photoelectrolysis and physical-properties of semiconducting electrode WO_2. *J. Appl. Phys.* **1977**, *48*, 1914–1920.

© 2014 by the authors; licensee MDPI, Basel, Switzerland. This article is an open access article distributed under the terms and conditions of the Creative Commons Attribution license (http://creativecommons.org/licenses/by/4.0/).